LINC00473 modulates protein expression to promote ovarian cancer progression and overcome cisplatin resistance

CAIRONG ZHANG[1,2], JIE MA[1,2], WENLING WANG[1,2], MIN GUO[1,2], CUILIU HAN[1,2], MADINAMU SADIKE[1,2] and KAICHUN ZHU[1,2]

[1]Department of Gynecology, People's Hospital of Xinjiang Uygur Autonomous Region, Ürümqi, Xinjiang Uygur Autonomous Region 830000, P.R. China; [2]Xinjiang Cervical Cancer Prevention and Treatment Clinical Research Center, People's Hospital of Xinjiang Uygur Autonomous Region, Ürümqi, Xinjiang Uygur Autonomous Region 830000, P.R. China

Received May 7, 2025; Accepted October 1, 2025

DOI: 10.3892/ol.2026.15456

Abstract. The present study aimed to systematically investigate the biological role of the long non-coding RNA (lncRNA) LINC00473 in the pathogenesis and progression of ovarian cancer and to explore its potential as a novel therapeutic target for clinical translation. LINC00473 expression was specifically silenced in SK-OV-3 and A2780 ovarian cancer cell lines using small interfering RNA technology. Enhanced Cell Counting Kit-8 and Transwell invasion assays were performed to evaluate the regulatory effects of LINC00473 on malignant phenotypes (proliferation, migration, invasion and apoptosis) and chemosensitivity to cisplatin (CDDP). Western blotting was utilized to detect changes in the expression levels of apoptosis-related proteins [poly (adenosine diphosphate-ribose) polymerase (PARP) and caspase-3] and stemness/drug resistance-associated proteins [Sox2 and Yes-associated protein 1 (YAP1)]. Knockdown of LINC00473 significantly inhibited ovarian cancer cell proliferation (SK-OV-3, 23.1%, P<0.001; A2780, 41.5%, P<0.001) and induced apoptosis (apoptosis rate 18.0-25.2%; P<0.001), while reducing migration and invasion by 30.7-55.4% and 31.9-54.5% (both P<0.001), respectively, accompanied by pseudopodia retraction and cellular rounding. At the molecular level, LINC00473 knockdown upregulated PARP/caspase-3 expression (1.7- and 2.3-fold) and downregulated Sox2/YAP1 (0.5- and 0.6-fold), with A2780 cells exhibiting 25% higher sensitivity to intervention compared with SK-OV-3 cells. Combined with CDDP treatment, the proliferation rate of A2780 further decreased to 35.5% (P<0.001). These findings indicate that LINC00473 may promote ovarian cancer progression by suppressing apoptosis and activating oncogenic pathways (Sox2/YAP1). Furthermore, silencing LINC00473 synergistically enhanced CDDP efficacy, particularly in A2780 cells exhibiting heightened sensitivity. These findings suggest that targeting LINC00473 may represent a novel therapeutic strategy for ovarian cancer; however further exploration of its molecular network and *in vivo* validation are warranted in the future.

Correspondence to: Dr Kaichun Zhu, Department of Gynecology, People's Hospital of Xinjiang Uygur Autonomous Region, 91 Tianchi Road, Tianshan, Ürümqi, Xinjiang Uygur Autonomous Region 830000, P.R. China
E-mail: zkc71@163.com

Key words: ovarian cancer, LINC00473, cisplatin resistance, cell proliferation, apoptosis

Introduction

Ovarian cancer is the most lethal of gynecological malignancies, with >70% of cases diagnosed at advanced stages. Due to delayed detection and both intrinsic and therapy-induced chemoresistance, ovarian cancer has a 5-year survival rate of <50% (1). Despite incremental advancements in cytoreductive surgery and platinum-based treatment protocols, recurrence and refractory disease continue to pose notable challenges, highlighting the urgent need for innovative therapeutic targets and strategies (2).

Previously, long non-coding RNAs (lncRNAs) have emerged as key regulators of oncogenesis, coordinating key cancer hallmarks including sustained proliferation, migration, invasion and drug resistance, through epigenetic, transcriptional and post-translational mechanisms (3-5). Among lncRNAs, LINC00473, a conserved oncogenic lncRNA, has been implicated in enhancing tumor aggressiveness and chemoresistance in lung, breast and hepatocellular carcinoma by disrupting key signaling pathways, such as the Hippo/Yes-associated protein (YAP) axis and Sox2-mediated stemness program (6-8). These pathways are essential for maintaining the plasticity of cancer stem cells (CSC) and DNA damage repair capacity, which are key factors determining platinum resistance in ovarian cancer (9-11).

In ovarian cancer, the role of LINC00473 remains largely unexplored. Research has indicated that lncRNAs serve a pivotal role in the progression and chemoresistance of ovarian cancer, highlighting their potential as therapeutic targets (12-14). For example, lncRNAs such as metastasis-associated lung adenocarcinoma transcript 1 (MALAT1) and HOX transcript antisense RNA (HOTAIR) have been demonstrated to facilitate ovarian cancer cell proliferation and to confer cisplatin (CDDP) resistance through diverse mechanisms (6-8). Nonetheless, the precise function of LINC00473 in ovarian

cancer progression and its viability as a therapeutic target have yet to be comprehensively studied.

While the mechanistic roles of certain lncRNAs such as MALAT1 and HOTAIR have been mechanistically associated with ovarian cancer progression and CDDP resistance, the functional landscape of LINC00473 in this malignancy remains largely unexplored. Based on its established roles in CSC maintenance and therapy resistance across other types of cancer such as non-small cell lung cancer (11), it may be hypothesized that LINC00473 drives ovarian cancer progression by enhancing proliferative capacity, metastatic potential and CDDP tolerance through Sox2/YAP1-dependent signaling. To address this knowledge gap, the present study aimed to investigate the direct effects of LINC00473 on key malignant phenotypes in two ovarian cancer cell lines, including proliferation, invasion, apoptosis and CDDP resistance. Furthermore, the underlying molecular mechanisms were preliminarily explored by analyzing Sox2/YAP1 protein expression levels using western blotting, providing initial evidence for the proposed signaling involvement. This integrated approach sought to characterize both the phenotypic impact of LINC00473 and potentially establish a foundation for further mechanistic dissection in future research.

Materials and methods

Cell culture and transfection. SK-OV-3 and A2780 ovarian cancer cells, obtained from Procell Life Science & Technology Co., Ltd. and iCell Bioscience Inc. companies respectively, were routinely cultured in McCoy's 5A medium (cat. no. PM150710; Procell Life Science & Technology Co., Ltd.) supplemented with 10% FBS (cat. no. FCS500; Shanghai ExCell Biology, Inc.) and Neomycin Solution Stabilized (cat. no. P477894; 1:100; Shanghai Aladdin Biochemical Technology Co., Ltd.). The cells were maintained under conditions of 37˚C, 5% CO_2 and 98% relative humidity, growing as a monolayer adherent to the culture surface. Once the cells reached 80-90% confluence, they were digested with 0.25% trypsin (cat. no. PB180226; Procell Life Science & Technology Co., Ltd.) and collected during the logarithmic growth phase.

To enhance the inhibitory effect on LINC00473, the knockdown of LINC00473 by using three small interfering RNA (siRNA, GuangZhou Ribobio Co., Ltd.) sequences simultaneously targeting distinct regions of its gene sequence (sequences listed in Table I). During transfection, the transfection reagent Lipofectamine® 2000 (cat. no. 11668019; Invitrogen; Thermo Fisher Scientific, Inc.) was used to deliver chemically synthesized siRNAs into ovarian cancer cells at a final siRNA concentration of 50 nM. The transfection mixture was incubated with cells at 37°C in a humidified atmosphere containing 5% CO_2 for 6 h, after which the medium was replaced with fresh complete medium. The transfection reagent facilitated the formation of RNA-lipid complexes, which mediated the delivery of siRNA into cells. The siRNA particularly bound to complementary sequences in LINC00473, leading to its cleavage and degradation via the RNA-induced silencing complex pathway, thus reducing its expression levels.

The experiment was divided into three groups: i) si-negative control (siNC) group (transfected with non-targeting scrambled siRNA); ii) siLINC00473 group (transfected with LINC00473-specific siRNA); and iii) untreated control group (untransfected cells). At 6 h post-transfection, the medium was replaced with fresh complete medium and the cells were cultured for a further 48 h. Each group included three replicate (wells) and the entire experiment performed as three independent biological replicates. Cells in the logarithmic growth phase (70-80% confluence) were collected for subsequent analyses.

LINC00473 knockdown efficiency analysis by reverse transcription-quantitative (q) PCR. Cells in the logarithmic growth phase were collected 48 h post-transfection from the following three groups: i) siNC group; ii) siLINC00473 group; and iii) untreated control group. Cells were washed twice with ice-cold PBS, then lysed in 1 ml/well TRIzol® reagent (cat. no. 15596026; Invitrogen; Thermo Fisher Scientific, Inc.) in a 6-well plate. Total RNA was extracted using chloroform-isopropanol precipitation and resuspended in RNase-free water. RNA concentration and purity (A260/A280 ratio, 1.8-2.1) were verified using a NanoDrop spectrophotometer (Thermo Fisher Scientific, Inc.).

Total RNA (1 μg) was then reverse-transcribed using the PrimeScript™ RT Master Mix kit (Takara Biotechnology Co., Ltd.) in a 20-μl reaction, which included a genomic DNA removal step (37˚C for 2 min) followed by cDNA synthesis (37˚C for 15 min and 85˚C for 5 sec). qPCR was performed using SYBR Premix Ex Taq™ (Takara Biotechnology Co., Ltd.) in a 10 μl reaction containing 0.4 μM each primer (sequences listed in Table I) and 2 μl cDNA (1:10 dilution). The cycling conditions were as follows: 95˚C for 30 sec, followed by 40 cycles of 95˚C for 5 sec and 60˚C for 30 sec. Melt curve analysis (65-95˚C, increment 0.5˚C/sec) confirmed single-peak amplification (15). The relative expression level of LINC00473 was normalized to GAPDH using the $2^{-\Delta\Delta Cq}$ method.

Cell Counting Kit 8 (CCK-8) assay. Logarithmic-phase cells from the siNC group, siLINC00473 group and untreated control group were trypsinized and resuspended in complete medium. Cells were then seeded in a 96-well plate at a density of $2.0x10^4$ cells/well, with five technical replicates per group. An additional cell-free blank control (100 μl complete medium only) was included to measure background absorbance. The outer wells of the plate were filled with 200 μl PBS to minimize edge effects.

Enhanced CCK-8 assays were performed at 24, 48, 72 and 96 h post-seeding. At each time point, the culture medium was aspirated and 100 μl fresh complete medium containing 10 μl CCK-8 reagent (cat. no. E-CK-A362; Wuhan Elabscience Biotechnology Co., Ltd.) was added to each well (final volume, 110 μl/well). The plate was incubated at 37˚C in the dark for 2 h. Absorbance (OD value) at 450 nm was measured using a microplate reader (BioTek Synergy HTX; BioTek; Agilent Technologies, Inc.). Cell viability (%) was calculated using the following formula: $[(OD_{experimental}-OD_{blank})/(OD_{control}-OD_{blank})]$ x100%. A proliferation curve was generated by plotting cell viability (%) on the y-axis against time points on the x-axis.

Cell migration and invasion assays. Logarithmic-phase cells were washed twice with PBS, digested with 0.25% trypsin at 37˚C for 2-3 min and resuspended in culture medium to a

Table I. siRNA sequences and qPCR primers information.

Gene	Primer	Sequence (5'-3')	PCR Products
siRNA targeting LINC00473	S1	GCACUUCCAGGAACAUCAU	-
	S2	GCUUCCAUUGCUGGAGCUU	-
	S3	GCCUGGUUGUUGGCAAGUA	-
Homo sapiens LINC00473	Forward	TGCAAAGCGGACACCTAGTA	215 bp
	Reverse	TTCTCCAGTTACCACCCACC	
Homo sapiens GAPDH	Forward	TCAAGAAGGTGGTGAAGCAGG	115 bp
	Reverse	TCAAAGGTGGAGGAGTGGGT	

qPCR, quantitative PCR; siRNA, small interfering RNA; LINC, long non-coding RNA.

density of $1.0x10^6$ cells/ml. For the migration assay, 200 μl cell suspension in serum-free medium (0% FBS) was added to the upper chamber of the Transwell insert, while 600 μl of medium containing 10% FBS (cat. no. 10099-141C; Gibco; Thermo Fisher Scientific, Inc.) was added to the lower chamber.

For the invasion assay, Matrigel (cat. no. 356234; Corning, Inc.) was thawed overnight at 4˚C and diluted with serum-free medium at a 1:8 ratio (v/v) on ice. A total of 40 μl of diluted Matrigel was evenly applied to the upper surface of the Transwell membrane (pore size, 8.0 μm; Corning, Inc.) using a pre-chilled pipette tip. The chamber was then incubated at 37˚C for 5 h for gel polymerization (confirmed by inverted microscopy). Unpolymerized Matrigel was aspirated gently before cell seeding.

Non-migrated/invaded cells on the upper surface were removed with a cotton swab after the cells were incubated at 37˚C in a humidified atmosphere with 5% CO_2 for 24 h. Migrated/invaded cells on the lower surface were fixed with 70% ice-cold ethanol at 4˚C for 15 min, washed twice with PBS and stained with 0.5% crystal violet in 25% methanol at room temperature for 20 min. Excess stain was removed by rinsing three times with distilled water and chambers were air-dried. Migrated or invaded cells were counted in five random fields per chamber at x200 magnification using a light microscope. Images were analyzed with ImageJ (version 1.8.0; National Institutes of Health) by thresholding and particle analysis.

Flow cytometric analysis of apoptosis. Adherent cells were detached using 0.25% trypsin (37˚C; 2 min) and digestion was terminated by adding complete medium containing 10% FBS. The cell suspension was washed twice with ice-cold PBS (300 x g, 5 min) and lastly resuspended in 1X Annexin V Binding Buffer (cat. no. GK10037; Shanghai HongYe Biotech Co., Ltd.) to a density of $1x10^6$ cells/ml. This concentration was experimentally determined to prevent cell aggregation during staining while maintaining sufficient event counts for statistical analysis. Aliquots of 100 μl (~$1x10^5$ cells) were transferred to 1.5-ml microcentrifuge tubes, to which 5 μl Annexin V-FITC conjugate and 5 μl PI stock solution (50 μg/ml in PBS) were added sequentially. The tubes were gently vortexed for 3 sec and incubated in the dark at room temperature for precisely 15 min, with periodic inversion every 5 min to ensure uniform dye distribution. Following incubation, Binding Buffer was added to each tube to terminate staining.

To ensure accurate gating and compensation, three control samples were processed in parallel: Negative control (unstained cells), single-stained controls (Annexin V or PI only) and positive control (apoptosis-induced cells). Flow cytometric detection was performed using a BriCyte E6 flow cytometer (Mindray). Data analysis was conducted with MR Flow software (version 3.0.2, Mindray) to quantify apoptotic cells. Flow cytometry parameters were set to detect FITC (Ex 488 nm/Em 530 nm) and PI (Ex 488 nm/Em 617 nm). Compensation values were adjusted using the single-stained controls: 5-10% from FITC to PI channel and 1-3% from PI to FITC channel to correct for fluorescence spillover. Data analysis distinguished live cells (Annexin V^-/PI^-), early apoptotic (Annexin V^+/PI^-) and late apoptotic/necrotic (double-positive) populations and total apoptosis rate (%) was calculated as follows: (Early+late apoptotic cells) / total cells x 100%. All steps were performed under light-protected conditions and detection was completed within 1 h after staining to ensure reliability.

Western blot analysis. Transfected cells were harvested by scraping in ice-cold PBS, followed by two washes to remove residual medium. Cell pellets were lysed in RIPA buffer (cat. no. P0013B; Beyotime Institute of Biotechnology) supplemented with protease/phosphatase inhibitors cocktail (1X final concentration; cat. no. 78440; Thermo Fisher Scientific, Inc.) on ice for 30 min with intermittent vortexing (every 10 min). Lysates were clarified by centrifugation at 14,000 x g for 15 min at 4˚C, and supernatants were transferred to pre-chilled 1.5 ml tubes. Protein concentration was determined using a BCA assay kit (cat. no. 23225; Thermo Fisher Scientific, Inc.) according to the manufacturer's instructions, with BSA (cat. no. G3522; GBCBIO Technologies, Inc.) as a standard. Samples were adjusted to 2 μg/μl with lysis buffer, mixed with 5X SDS loading buffer to a final 1X concentration and denatured at 95˚C for 5 min.

Proteins were separated by SDS-PAGE gels (1.5 mm thick) with 4% stacking gels. Samples (20-40 μg protein per lane, quantified by BCA assay) were electrophoresed at 120 V for 1.5 h in standard running buffer. Following separation, the proteins were transferred to polyvinylidene fluoride membranes (0.45 μm) using wet transfer at 300 mA for 90 min in transfer buffer containing 20% methanol. Transfer efficiency was verified by Ponceau S staining (5 min) and destaining.

Membranes were blocked with 5% (w/v) non-fat dry milk in TBS with Tween-20 [TBST; 20 mM Tris-HCl (pH 7.5), 150 mM NaCl and 0.1% Tween-20] at room temperature for 1 h with gentle agitation. The following primary antibodies were diluted in antibody dilution buffer (5% BSA in TBST): Anti-caspase-3 (cat. no. 25128-1-AP; 1:1,000; Proteintech Group, Inc.), anti-cleaved-poly (adenosine diphosphate-ribose) polymerase (PARP; cat. no. bsm-52408R; 1:1,000; BIOSS), anti-YAP1 (cat. no. bs-3605R; 1:2,000; BIOSS), anti-Sox2 (cat. no. bs-0523R; 1:500; BIOSS) and anti-glyceraldehyde-3-phosphate dehydrogenase (GAPDH; cat. no. 60004-1-Ig; 1:5,000; Proteintech Group, Inc.). Membranes were incubated with primary antibodies overnight at 4˚C, followed by three 10-min washes in TBST. Horseradish peroxidase-conjugated goat anti-rabbit (cat. no. A0208; 1:5,000) and goat anti-mouse (cat. no. A0216; 1:5,000) IgG H&L secondary antibodies (both from Beyotime Institute of Biotechnology) were applied for 1 h at room temperature, followed by three additional TBST washes.

Chemiluminescent signals were detected using ECL substrate (cat. no. WBKLS0500; MilliporeSigma) and were captured with a ChemiDoc MP imaging system (Bio-Rad Laboratories, Inc.). Exposure times were optimized for each target protein (10 sec-10 min) to avoid signal saturation, with multiple exposures collected for dynamic range verification. Band intensities were semi-quantified using ImageLab software (version 6.1; Bio-Rad Laboratories, Inc.).

CDDP sensitivity assay. Ovarian cancer cells were divided into four groups (siNC, siLINC00473, siNC+30 μM CDDP and siLINC00473+30 μM CDDP), which were co-treated with CDDP (cat. no. 15663-27-1; MedChemExpress) for 48 h post-transfection and analyzed for cell viability using the CCK-8 assay. Briefly, culture medium was discarded, the cells were washed with PBS and fresh medium containing 10% CCK-8 reagent was add to each well and incubated at 37˚C in a humidified atmosphere with 5% CO_2 in the dark for 2 h. Lastly, the absorbance was measured at 450 nm using a microplate reader and the relative survival rate (% of control group) was calculated. Three independent replicates were performed to evaluate the cytotoxic effects of CDDP and the regulatory effect of LINC00473 silencing on drug sensitivity.

Statistical analysis. Relative cell proliferation was expressed as the mean OD_{450} (blank-corrected) at each time point. For CCK-8 relative cell viability (normalized to the siNC control), a two-way ANOVA evaluated the effects of siRNA treatment (siNC vs. siLINC00473) and CDDP exposure (0 vs. 30 μM), including their interaction. Data were normalized to the 24 h time point (set to 100%) to compare proliferation rates across the groups. All experiments were performed with three independent biological replicates. Data are presented as mean±SD from three replicates. Bar graphs display the mean±SD with individual data points and significant differences are marked as *P<0.05, **P<0.01, ***P<0.001. Statistical analyses were performed using GraphPad Prism (version 20.0; Dotmatics) with α=0.05 (two-tailed). Prior to selecting the statistical test, the normality of the data was assessed using Q-Q plot analysis. One-way/two-way ANOVA (with Tukey's post hoc test) was applied for data that conformed to a normal distribution, while the Kruskal-Wallis test was used for non-normal data. P<0.05 was considered to indicate a statistically significant difference.

Results

Expression level of the lncRNA LINC00473. To investigate the knockdown efficiency of siRNA targeting the lncRNA LINC00473, SK-OV-3 and A2780 ovarian cancer cell lines were transfected with siLINC00473 or siNC using a Lipofectamine-based transfection method. qPCR analysis revealed a significant reduction in LINC00473 expression in both cell lines transfected with siLINC00473. Compared with that in the siNC and blank control groups, LINC00473 expression was decreased by 27.01±4.70% (P<0.01, Fig. 1A) in SK-OV-3 cells and 42.96±4.39% (P<0.01, Fig. 1B) in A2780 cells, with statistically significant differences. Notably, the knockdown efficiency demonstrated no notable variation between the two cell lines, indicating the broad applicability of siRNA-mediated LINC00473 suppression.

Cell proliferation and apoptosis. Time-course analysis demonstrated that siLINC00473 transfection induced progressive and duration-dependent suppression of the proliferative activity of both SK-OV-3 and A2780 ovarian cancer cells. Significant inhibition emerged at 48 h post-transfection compared with in the siNC and untreated control groups (Fig. 2A and B). At this time point, SK-OV-3 cells retained 85.61% relative proliferative activity (14.39% suppression rate, P<0.001), while A2780 cells exhibited markedly stronger suppression, with 48.34% residual proliferative activity (51.66% suppression rate, P<0.001). By 72 h, SK-OV-3 suppression further intensified, with the suppression rate increased to 19.59% (P<0.001), whereas A2780 cells exhibited no additional suppression, stabilizing at 48.66% suppression rate (P<0.001). At the 96 h endpoint, suppression rate plateaued at 23.14% for SK-OV-3 (P<0.001) and 41.51% for A2780 cells (P<0.001). These findings indicated the specific anti-proliferative efficacy of siLINC00473 in ovarian cancer models (Fig. 2C).

siLINC00473-induced apoptosis in ovarian cancer cells exhibited time-dependent dynamics and was synchronized with cell proliferation inhibition (Figs. 2D, S1A and S1B). During the 48 h early apoptotic phase (E), the apoptosis rate of SK-OV-3 cells was 11.66±0.27%, significantly higher compared with that of the siNC group (4.45±0.14%; P<0.001), accompanied by a proliferation inhibition rate of 14.39±1.23%. A2780 cells displayed a similar apoptotic response (Figs. 2E, S1C and S1D), with an apoptosis rate of 12.33±0.23% (vs. siNC group, 2.84±0.11%; P<0.001), while its proliferation inhibition rate reached 51.66%±0.68%. By the 72 h late apoptotic phase (L), the apoptosis rate of SK-OV-3 decreased to 6.36±0.52%, remaining significantly higher compared with that in the siNC group (3.01±0.34%; P<0.001), yet its proliferation inhibition rate increased to 19.59±1.85%. By contrast, A2780 cells maintained a high apoptosis rate (12.90%±0.10%, vs. siNC group, 3.18±0.17%; P<0.001), although its proliferation inhibition rate slightly declined to 48.66±4.13%. Total apoptosis rates (E+L; T) revealed that SK-OV-3 cells reached 18.02±0.76% and A2780 cells 25.23±0.15%, both significantly higher compared with their respective control groups (SK-OV-3 control, 7.45±0.41%; P<0.001; A2780 control, 6.02±0.24%; P<0.001).

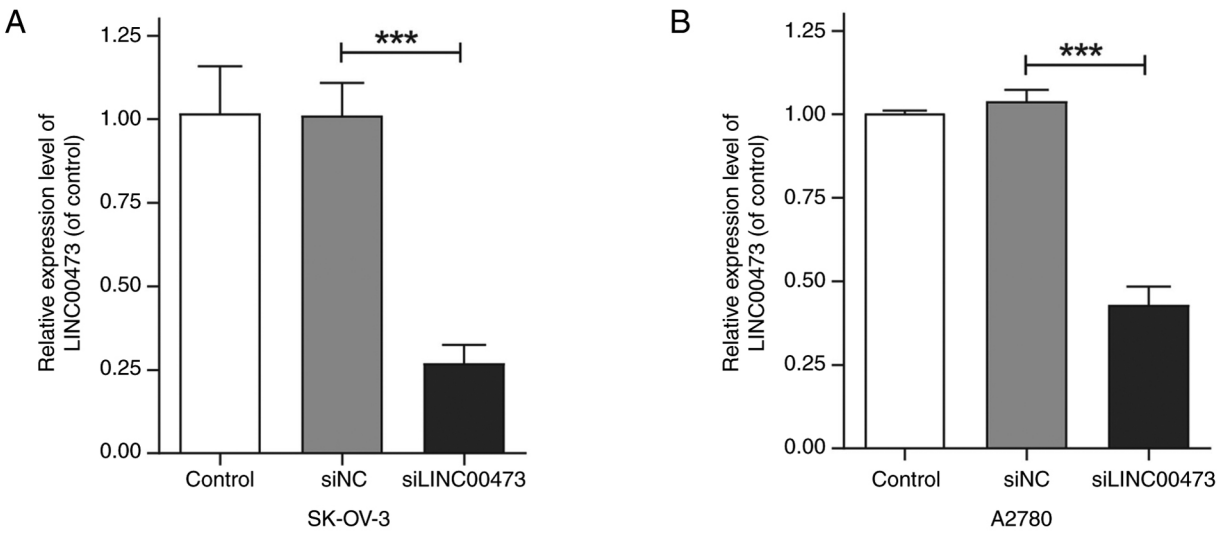

Figure 1. LINC00473 knockdown efficiency in ovarian cancer cell lines. Quantitative analysis of LINC00473 expression in (A) SK-OV-3 and (B) A2780 cells after transfection with siLINC00473, compared with siNC and untreated controls. Data are presented as the mean±SD. ***P<0.001. LINC, long non-coding RNA; NC, negative control; si, small interfering RNA.

While apoptosis and proliferation inhibition rates in both cell lines increased over time, A2780 cells demonstrated higher sensitivity to siLINC00473, as evidenced by its elevated total apoptosis and proliferation inhibition rates compared with SK-OV-3 cells.

Suppression of cell migration and invasion. To investigate the regulatory role of LINC00473 in ovarian cancer metastasis, the present study systematically analyzed cell migration and invasion phenotypes using Transwell assays. The results demonstrated that transfection with siLINC00473 significantly suppressed both migratory and invasive capacities in the two ovarian cancer cell lines (Fig. 3).

In SK-OV-3 cells (Fig. 3B and E), the migratory cell count decreased from 113.3±1.2 cells/field in the siNC group to 79.7±5.9 cells/field (30.71% inhibition; P<0.001), while the invasive cell count dropped from 95.0±2.6 to 64.7±4.0 cells/field (31.93% suppression; P<0.001). A2780 cells exhibited even more pronounced inhibition (Fig. 3C and F): Migratory cell numbers sharply declined from 287.7±5.5 to 128.3±6.5 cells/field (55.39% reduction; P<0.001) and invasive cell counts decreased from 187.7±5.5 to 85.3±5.5 cells/field (54.53% attenuation; P<0.001).

Microscopic imaging (x200 magnification) revealed a marked reduction in membrane, traversing cell density in the siLINC00473-transfected groups, accompanied by pseudopodia retraction and a rounded cellular morphology (Fig. 3A and D). Statistical analyses further confirmed that A2780 cells demonstrated a 25% higher sensitivity to LINC00473 silencing compared with SK-OV-3 cells, as evidenced by the differential inhibition rates in both migration and invasion. These findings collectively highlighted the key role of LINC00473 in regulating the metastatic behaviors of ovarian cancer cells.

Regulation of apoptosis and oncogenic proteins. Western blot analysis (Fig. 4A) revealed that transfection with siLINC00473 significantly upregulated the expression levels of apoptosis-associated proteins PARP and caspase-3 (both P<0.001) compared with those in the siNC group, while markedly suppressing the protein levels of stemness and metastasis-related markers Sox2 and YAP1 (both P<0.001). Semi-quantitative normalization to GAPDH (Fig. 4B-E) demonstrated that the PARP/GAPDH ratio in SK-OV-3 and A2780 cells increased to 1.76±0.15-fold and 2.25±0.25-fold of the control group, respectively. Similarly, caspase-3/GAPDH ratios rose to 1.66±0.08-fold (SK-OV-3) and 2.02±0.09-fold (A2780), indicating robust activation of apoptotic pathways upon LINC00473 silencing (Fig. 4B and C).

Concurrently, Sox2 and YAP1 expressions exhibited consistent yet quantitatively distinct inhibition across the two cell lines (Fig. 4D and E). In SK-OV-3 cells, Sox2/GAPDH and YAP1/GAPDH ratios decreased to 0.61±0.05-fold and 0.58±0.05-fold of the control, respectively. A2780 cells demonstrated more pronounced reductions, with Sox2 and YAP1 levels dropping to 0.49±0.04-fold and 0.60±0.03-fold of the control. These findings align with the aforementioned migration and invasion assays. The coordinated suppression of stemness/metastasis markers and activation of apoptosis further supports a dual regulatory mechanism underlying the role of LINC00473 in ovarian cancer progression.

Enhanced CDDP sensitivity. Under CDDP treatment, both ovarian cancer cell lines transfected with siLINC00473 exhibited significantly reduced viability compared with that in the siNC group (both P<0.001), with a time-dependent inhibitory effect. In SK-OV-3 cells (Fig. 5A), the relative proliferation rate of the siLINC00473+CDDP combination group progressively declined over time: 52.77±2.19% at 24 h, 43.19±0.39% at 48 h, 37.30±1.22% at 72 h, and 37.71±0.71% at 96 h, all significantly lower compared with the siNC group (P<0.001). Although the siNC+CDDP group indicated stronger antiproliferative effects compared with siLINC00473 monotherapy, its impact remained weaker compared with the combination group, while still being significantly suppressed compared with siNC (P<0.001).

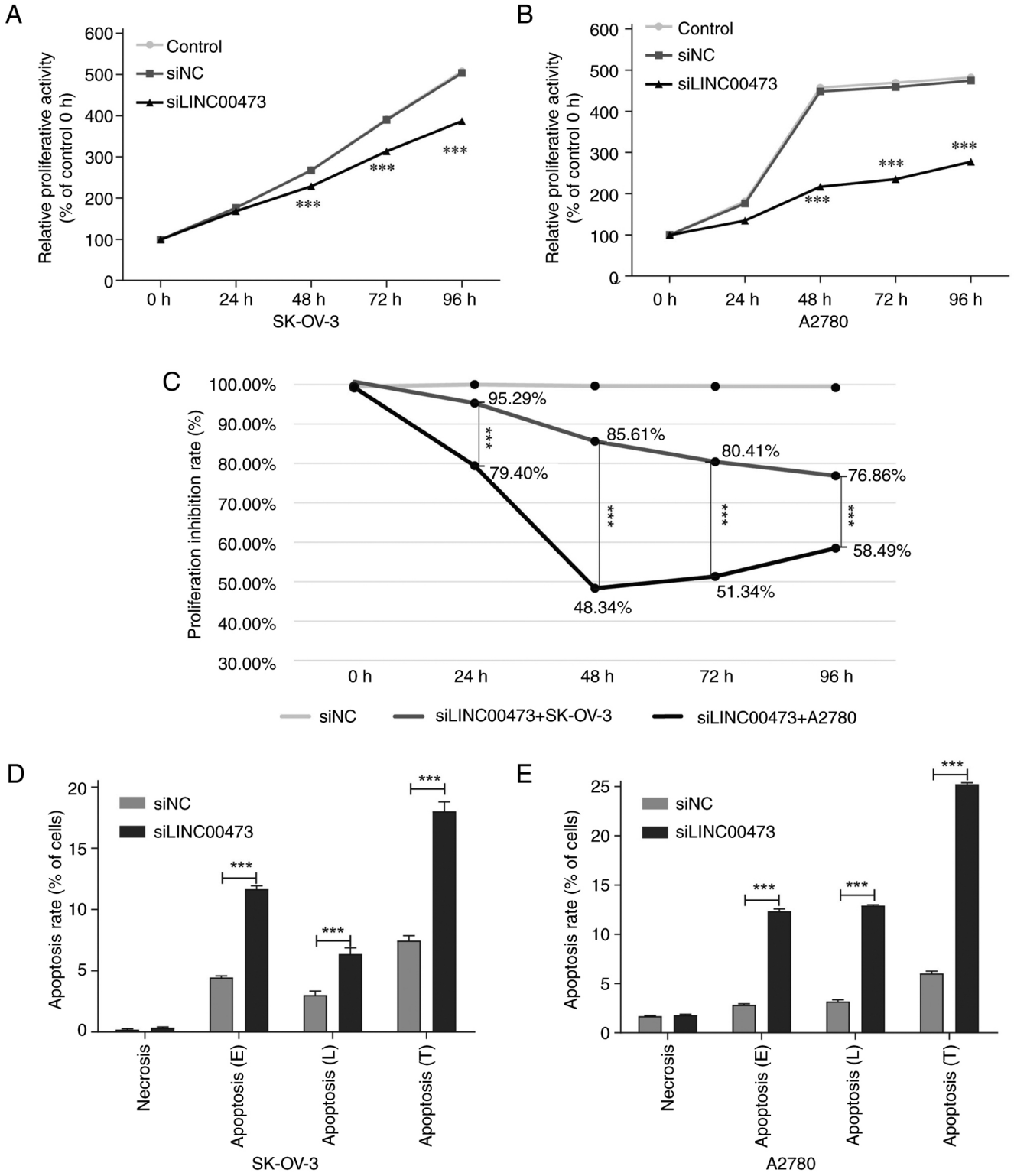

Figure 2. Silencing LINC00473 significantly inhibits cell proliferation and induces apoptosis. Proliferation of (A) SK-OV-3 and (B) A2780 cells after transfection with siLINC00473, siNC and untreated controls (C). Proliferation inhibition rates of both cell lines post-transfection. Apoptosis status of (D) SK-OV-3 and (E) A2780 cells. Data are presented as the mean±SD. ***P<0.001. LINC, long non-coding RNA; NC, negative control; si, small interfering RNA.

In A2780 cells (Fig. 5B), the inhibitory effects of the combined treatment were more pronounced. Compared with in the siNC group, the siLINC00473+CDDP group displayed a proliferation rate of 71.39±1.47% at 24 h, followed by a sharp decline to 38.99±1.98% at 48 h and further reductions to 37.82±0.35% at 72 h and 35.55±1.54% at 96 h (P<0.001). Both the siNC+CDDP group and siLINC00473 monotherapy group significantly suppressed proliferation (both P<0.001), but their effects were less potent compared with the combination treatment. These results indicated that LINC00473 silencing may synergize with CDDP to induce time-enhanced antitumor activity, with the inhibitory effects becoming particularly prominent after 48 h.

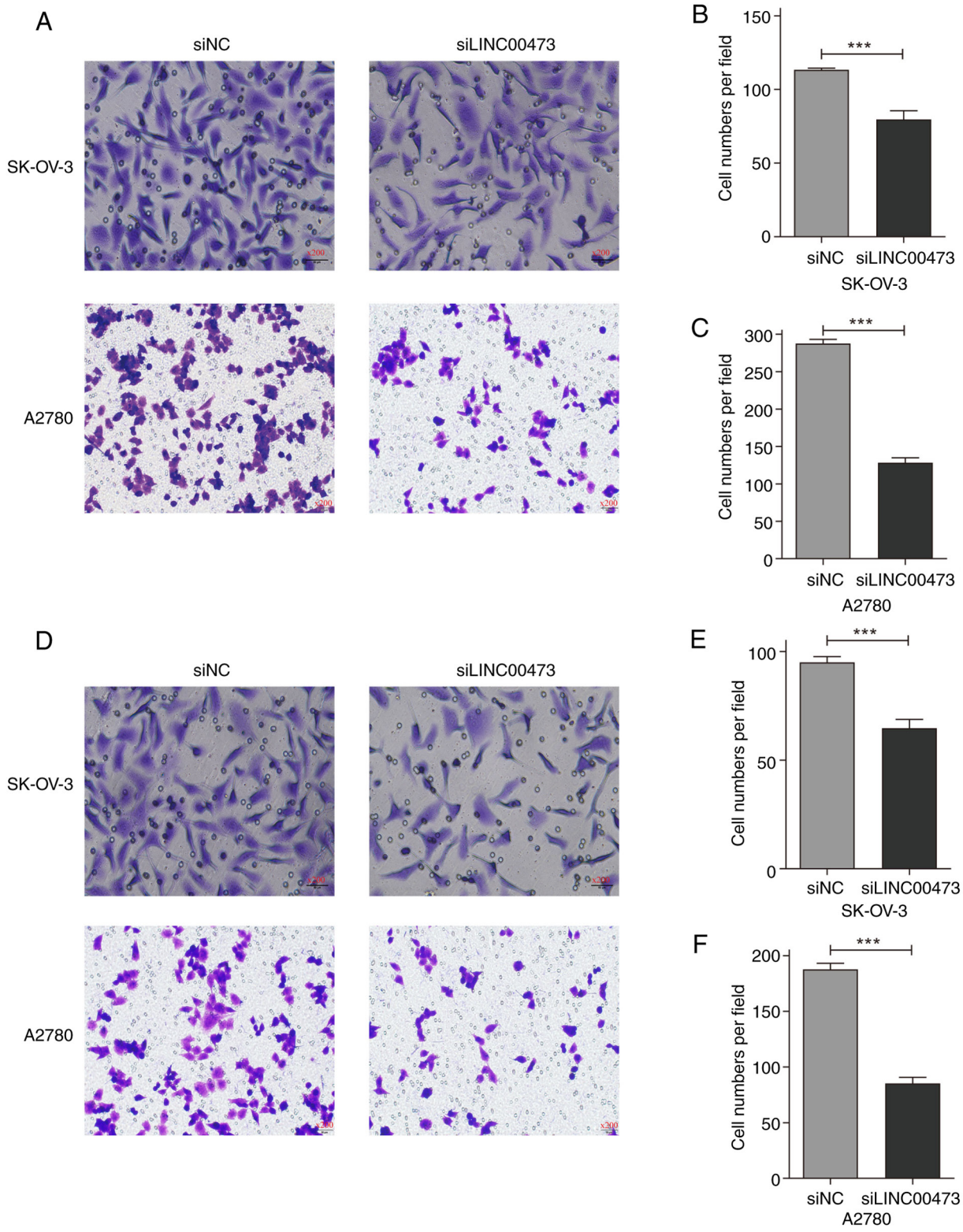

Figure 3. Cell migration and invasion after siLINC00473 transfection. Transfection of siLINC00473 markedly reduced both (A-C) migration and (D-F) invasion of ovarian cancer cells compared with those transfected with siNC. Representative crystal violet-stained microscopic images (x200 magnification) illustrate the (A) migrated and (D) invaded cells, with quantitative analyses confirming statistically significant inhibition of (B and C) migration and (E and F) invasion. Data are presented as mean±SD; ***P<0.001. LINC, long non-coding RNA; NC, negative control; si, small interfering RNA.

Discussion

LINC00473 is a lncRNA that is aberrantly upregulated in various malignancies, including pancreatic cancer, liver cancer and pituitary adenoma. LINC00473 expression level is markedly associated with tumor invasion, metastasis and poor patient prognosis, making it a potential pan-cancer biomarker (16,17). Previous studies have reported that LINC00473 regulates tumor cell malignancy through a competitive endogenous RNA (ceRNA) mechanism by sponging

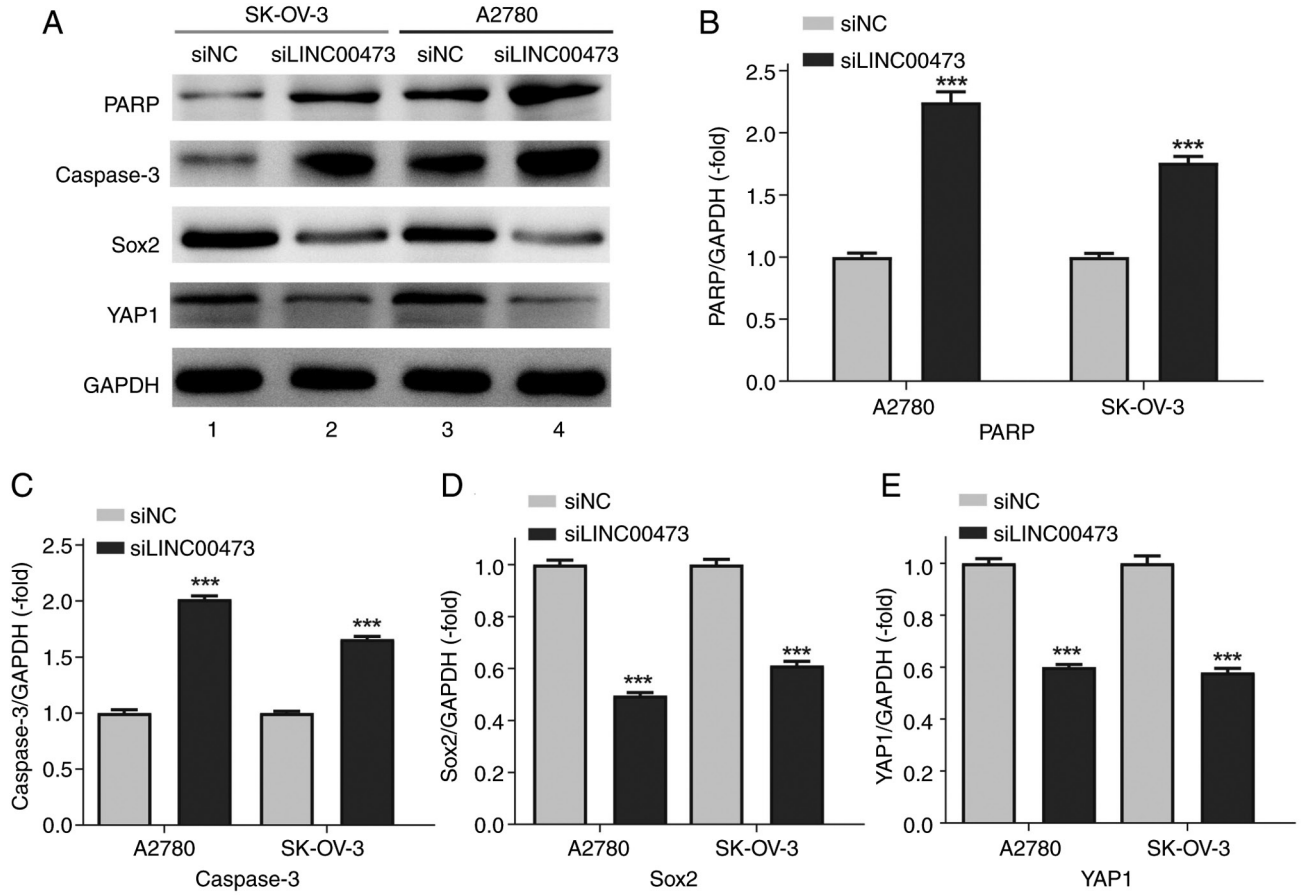

Figure 4. Cellular protein expression after siLINC00473 transfection. (A) Differential expression patterns of five proteins in two ovarian cancer cell lines after transfection with siLINC00473 vs. the scrambled siNC. Semi-quantitative analysis of relative expression levels of (B) PARP, (C) caspase-3, (D) Sox2 and (E) YAP1 normalized to GAPDH, demonstrating significant downregulation in siLINC00473-treated cells compared with siNC. Data are presented as the mean±SD; ***P<0.001. LINC, long non-coding RNA; NC, negative control; PARP, poly (adenosine diphosphate-ribose) polymerase; si, small interfering RNA; YAP1, yes-associated protein 1.

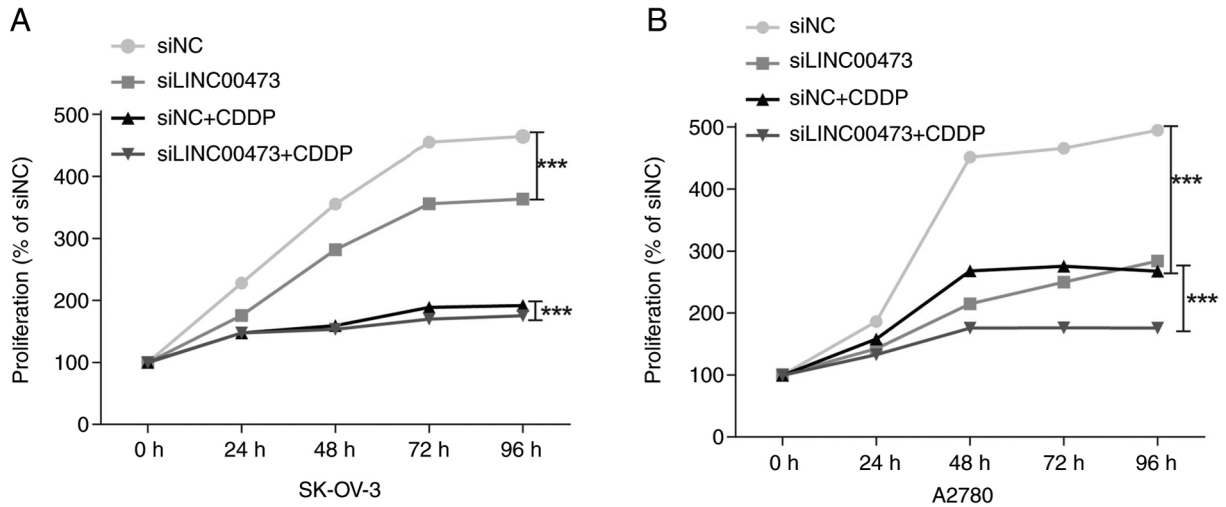

Figure 5. Effect of siLINC00473 transfection on cellular sensitivity to CDDP. Comparison of cellular sensitivity to CDDP after transfection of (A) SK-OV-3 and (B) A2780 cells with siLINC00473, compared with the siNC group and the blank control group. ***P<0.001. LINC, long non-coding RNA; CDDP, cisplatin; NC, negative control; si, small interfering RNA.

microRNAs (miRNAs/miRs) (18), such as miR-502-3p (19), miR-424-5p (20) and miR-497-5p (21), thereby alleviating miRNA-mediated suppression of downstream target genes. Furthermore, LINC00473 interacts with proteins such as phosphatidylethanolamine-binding protein 1 to indirectly promote tumor proliferation by inhibiting key signaling

pathways (22-24). The present study focused on ovarian cancer. Although not directly involving miRNA research, silencing LINC00473 revealed its biological functions: Suppression of LINC00473 significantly inhibited ovarian cancer cell proliferation, migration and invasion, which was closely associated with apoptosis activation (PARP cleavage and caspase-3 activation) and downregulation of CSC-related proteins (Sox2 and YAP1). Notably, LINC00473 silencing significantly enhanced ovarian cancer cell sensitivity to CDDP, suggesting its potential role in modulating pathways such as DNA damage repair to influence chemotherapy efficacy.

Liposome transfection achieved significant silencing of LINC00473 in SK-OV-3 and A2780 ovarian cancer cell lines, with significant differences in silencing efficiency between SK-OV-3 (27.01%) and A2780 (42.96%). However, this efficiency contrasts with higher lncRNA silencing rates reported in other studies. For example, siRNA-mediated knockdown of lncRNA HULC in liver cancer has been reported to achieve 52-70% efficiency (25) and siRNA targeting lncRNA HOTAIR in SK-OV-3 demonstrated 51% knockdown efficiency (26), both markedly surpassing the 27.01% observed in SK-OV-3 cells in the present study. This discrepancy may stem from the use of lentiviral infection in the aforementioned previous studies, which yield higher silencing efficiency compared with liposome-based methods. Notably, the differential silencing efficiency between SK-OV-3 and A2780 cells may arise from the distinct molecular characteristics of the two cell lines. The elevated expression levels of stemness markers such as CD133 in A27804 cells could enhance cellular dependency on LINC00473, thereby increasing susceptibility to silence interventions (27).

Following transfection, siLINC00473 significantly inhibited the proliferation of SK-OV-3 and A2780 cells. The rapid response in A2780 cells (48 h inhibition rate, 51.67%) aligns with previous reports of high sensitivity to lncRNA-dependent proliferation in aggressive ovarian cancer cells (28-30), while the later stagnation in inhibition may be associated with limitations of *in vitro* culture conditions (such as nutrient competition and microenvironment). By contrast, the delayed inhibition in SK-OV-3 (23.14% at 96 h) may stem from its inherently slower proliferation rate. The temporal synchronization between apoptosis rates and proliferation inhibition suggests that LINC00473 may coordinately regulate the proliferation-apoptosis balance. The higher apoptosis rate in A2780 cells could be associated with Bcl-2 family protein modulation, a phenomenon previously observed in lncRNA CCAT1 silencing models (31). Notably, A2780 cells exhibited stronger migration/inhibition suppression (~55%) compared with SK-OV-3 cells (~30%), possibly due to a greater dependency on epithelial-mesenchymal transition (EMT) phenotypes, analogous to the mechanism by which lncRNA colon cancer-associated transcript 2 promotes EMT via the Wnt/β-catenin pathway (32).

The present study demonstrated that silencing LINC00473 exerted a dual antitumor effect on ovarian cancer by activating apoptotic pathways and suppressing proteins associated with stemness and metastasis. Following LINC00473 knockdown, cleaved-PARP were significantly upregulated, consistent with the key roles of this proteins in regulating apoptosis (33). While activated caspase-3 was also evaluated in the present study, it is important to clarify that the level of cleaved caspase-3 was not actually assessed. Consequently, the activation status of cleaved caspase-3 cannot be directly determined, which represents a limitation of this study. Notably, the upregulation of cleaved-PARP strongly suggests activation of the apoptotic pathway, as this process is typically accompanied by caspase-3 cleavage. The primary finding, that silencing LINC00473 promotes ovarian cancer cell apoptosis, still aligns with previous studies associating LINC00473 to apoptotic regulation (20-22,34).

Simultaneously, the inhibition of Sox2 and YAP1 highlights the role of LINC00473 in modulating cancer stemness and metastasis. Sox2 serves as a pivotal pluripotent factor indispensable for sustaining the CSC population. It serves a key role in driving chemotherapy resistance and relapse in ovarian cancer (35). The present study revealed that silencing LINC00473 resulted in a significant decline in Sox2 levels, particularly in A2780 cells, where the levels were 0.49-fold lower compared with those in the control group. By downregulating Sox2, LINC00473 may effectively diminish the CSC subpopulation within ovarian tumors, leading to more efficient suppression of tumor growth and progression. Furthermore, based on the findings from the CDDP resistance study, it can be hypothesized that LINC00473 modulates the sensitivity of ovarian cancer cells to chemotherapeutic agents by regulating Sox2. When LINC00473 is silenced and Sox2 levels decrease, tumor cells may potentially become more vulnerable to the cytotoxic effects of chemotherapeutic drugs, ultimately enhancing treatment outcomes. The Hippo pathway effector, YAP1, contributes to metastatic dissemination by promoting EMT and stromal remodeling (36). The present study demonstrated that following LINC00473 knockdown, YAP1 underwent coordinated downregulation, with levels decreasing by 0.58-0.60-fold. This downregulation may impede EMT, curtail the migration and invasion of ovarian cancer cells and thus, inhibit tumor metastasis. Furthermore, it could disrupt the conducive tumor microenvironment that facilitates cancer progression and metastasis, thereby impacting the proliferation and survival of cancer cells.

The present study confirmed the synergistic antitumor effect of LINC00473 silencing combined with CDDP (siLINC00473+CDDP), which induced time-dependent proliferation inhibition in both SK-OV-3 and A2780 cells, with significantly enhanced efficacy after 48 h. These findings suggested that targeting LINC00473 may overcome adaptive chemoresistance in tumor cells, thereby sensitizing them to CDDP. The combination therapy outperformed monotherapy (siLINC00473 or CDDP alone) in both cell lines, particularly in A2780 cells, where the proliferation rate dropped to 38.99±1.98% (vs. siNC group) after 48 h, indicating time-accumulative synergy. This aligns with the clinical rationale for chemotherapy cycle design, where prolonged drug exposure amplifies therapeutic efficacy through cumulative molecular damage (37). Similar synergy has been reported in other lncRNA studies (38,39), for example, silencing lncRNA HOTAIR has been shown to enhance ovarian cancer cell sensitivity to paclitaxel via apoptosis pathway activation (40). Although both cell lines exhibited synergy, A2780 cells exhibited a more pronounced response (96 h proliferation rate, 35.55±1.54% vs. 37.71±0.71% in SK-OV-3 cells). This

discrepancy likely stems from tumor heterogeneity: A2780 cells, derived from a chemotherapy-naïve patient, exhibits lower intrinsic resistance, whereas SK-OV-3 cells, isolated from metastatic ascites, may possess stronger microenvironmental adaptability (41). This underscores the need for molecular subtyping to identify patient populations most likely to benefit from such combinatorial strategies in future clinical applications.

The present study revealed the key pro-tumorigenic role of LINC00473 in ovarian cancer and its potential as a therapeutic target. Experimental evidence demonstrated that silencing LINC00473 suppressed malignant progression through dual mechanisms: i) Activating the PARP/caspase-3 apoptosis pathway to induce cell death; and ii) downregulating Sox2 and YAP1 to inhibit CSC properties and metastasis-related phenotypes. Notably, LINC00473 silencing exhibited significant synergistic effects with CDDP treatment, particularly in chemotherapy-naïve A2780 cells, which exhibit heightened sensitivity. The differential responses across cell lines (including time-dependent proliferation inhibition and varying levels of migration/invasion suppression) reflect tumor heterogeneity and underscore the importance of molecular subtyping for personalized therapy. These findings not only validate the oncogenic function of LINC00473 but also reveal its regulatory network independent of the ceRNA mechanism, positioning it as a novel therapeutic target to inform clinical strategies for ovarian cancer in the future.

Although the present *in vitro* experiments have yielded valuable insights into the role of LINC00473 in ovarian cancer, the lack of *in vivo* validation results stems from limitations in project duration and funding. The *in vitro* experimental environment, by its nature, cannot fully and accurately replicate the intricate interplay among various factors within the complex human physiological milieu. Notably, the interference results of siLINC00473 have largely achieved the anticipated verification effect. Due to this, it is imperative to employ animal models in subsequent research to further investigate and confirm the current findings. Based on the current research findings, in future studies, knockdown/overexpression rescue experiments in combination with pathway inhibitors should be performed to thoroughly explore the direct interactions and specific molecular mechanisms between Sox2, YAP1 and LINC00473 in regulating the biological behavior of ovarian cancer cells, aiming to clarify their regulatory relationships. Furthermore, it is essential to perform a clinical evaluation of the therapeutic potential of treatment methods targeting LINC00473.

In conclusion, LINC00473 has emerged as a pivotal oncogenic lncRNA with multifaceted roles in ovarian cancer progression and therapy resistance. Its upregulation may drive tumor aggressiveness by orchestrating dual mechanisms: Apoptosis evasion (via PARP/caspase-3 suppression) and CSC maintenance (through Sox2/YAP1 upregulation). Silencing LINC00473 not only inhibited proliferation, migration and invasion but also synergized with CDDP, overcoming adaptive chemoresistance likely by impairing DNA damage repair pathways. The divergent responses between SK-OV-3 (metastatic, slower-proliferating) and A2780 (chemotherapy-naïve, aggressive) cells underscore the impact of tumor heterogeneity on therapeutic outcomes, emphasizing the need for molecular subtyping to tailor combinatorial strategies in the future.

Acknowledgements

The authors would like to thank Mr. Wenbo Zhao and Mr. Chaoyang Chen (both affiliated with Xinjiang Dingju Biotechnology Co., Ltd., Ürümqi, Xinjiang Uygur Autonomous Region, China) for their technical support in data analysis.

Funding

The present study was supported by Special Programme for the in-hospital Project of the People's Hospital of Xinjiang Uygur Autonomous Region (grant no. 20210210).

Availability of data and materials

The data generated in the present study may be requested from the corresponding author.

Authors' contributions

CZ and KZ conceived and designed the study. CH and MS collected the data. JM, WW and MG performed the analysis and interpretation of the data. CZ drafted the manuscript. MG and KZ revised the manuscript. WW and MG confirm the authenticity of all the raw data. All authors read and approved the final manuscript.

Ethics approval and consent to participate

Not applicable.

Patient consent for publication

Not applicable.

Competing interests

The authors declare that they have no competing interests.

References

1. Siegel RL, Miller KD, Wagle NS and Jemal A: Cancer statistics, 2023. CA Cancer J Clin 73: 17-48, 2023.
2. Lheureux S, Braunstein M and Oza AM: Epithelial ovarian cancer: Evolution of management in the era of precision medicine. CA Cancer J Clin 69: 280-304, 2019.
3. Bhan A, Soleimani M and Mandal SS: Long noncoding RNA and cancer: A new paradigm. Cancer Res 77: 3965-3981, 2017.
4. Zhang X, Wang W, Zhu W, Dong J, Cheng Y, Yin Z and Shen F: Mechanisms and functions of long non-coding RNAs at multiple regulatory levels. Int J Mol Sci 20: 5573, 2019.
5. Slack FJ and Chinnaiyan AM: The Role of non-coding RNAs in oncology. Cell 179: 1033-1055, 2019.
6. Li L, Zhang X, Liu N, Chen X and Peng C: LINC00473: A novel oncogenic long noncoding RNA in human cancers. J Cell Physiol 236: 4174-4183, 2021.
7. Yang WZ, Zhou H and Yan Y: XIAP underlies apoptosis resistance of renal cell carcinoma cells. Mol Med Rep 17: 125-130, 2018.
8. Yang L, Xie HJ, Li YY, Wang X, Liu XX and Mai J: Molecular mechanisms of platinum-based chemotherapy resistance in ovarian cancer (review). Oncol Rep 47: 82, 2022.

9. Zanconato F, Cordenonsi M and Piccolo S: YAP/TAZ at the roots of cancer. Cancer Cell 29: 783-803, 2016.
10. Chen Y, Li Z, Chen X and Zhang S: Long non-coding RNAs: From disease code to drug role. Acta Pharm Sin B 11: 340-354, 2021.
11. Mo J, Li B, Zhou Y, Xu Y, Jiang H, Cheng X, Wu X and Zhang Y: LINC00473 promotes hepatocellular carcinoma progression via acting as a ceRNA for microRNA-195 and increasing HMGA2 expression. Biomed Pharmacother 120: 109403, 2019.
12. Wang JY, Lu AQ and Chen LJ: LncRNAs in ovarian cancer. Clin Chim Acta 490: 17-27, 2019.
13. Shankaraiah RC, Veronese A, Sabbioni S and Negrini M: Non-coding RNAs in the reprogramming of glucose metabolism in cancer. Cancer Lett 419: 167-174, 2018.
14. Leeper NJ and Maegdefessel L: Non-coding RNAs: Key regulators of smooth muscle cell fate in vascular disease. Cardiovasc Res 114: 611-621, 2018.
15. Livak KJ and Schmittgen TD: Analysis of relative gene expression data using real-time quantitative PCR and the 2(-Delta Delta C(T)) method. Methods 25: 402-408, 2001.
16. Zhang Q, Wang G, Xu L, Yao Z and Song L: Long non-coding RNA LINC00473 promotes glioma cells proliferation and invasion by impairing miR-637/CDK6 axis. Artif Cells Nanomed Biotechnol 47: 3896-3903, 2019.
17. Zhu S, Fu W, Zhang L, Fu K, Hu J, Jia W and Liu G: LINC00473 antagonizes the tumour suppressor miR-195 to mediate the pathogenesis of Wilms tumour via IKKα. Cell Prolif 51: e12416, 2018.
18. Wang H, Gao L, Chen Y, Zhang L, Bai Y, Zhao C, Zhang L, Zuo L and Sun H: Identification of hub genes in bladder transitional cell carcinoma through ceRNA network construction integrated with gene network analysis. J Cell Mol Med 28: e17979, 2024.
19. Li J, Qian Y, Zhang C, Wang W, Qiao Y, Song H, Li L, Guo J, Lu D and Deng X: LncRNA LINC00473 is involved in the progression of invasive pituitary adenoma by upregulating KMT5A via ceRNA-mediated miR-502-3p evasion. Cell Death Dis 12: 580, 2021.
20. Zhang C and Yang T: Long Non-coding RNA LINC00473 promotes breast cancer progression via miR-424-5p/CCNE1 pathway. Protein Pept Lett 30: 72-84, 2023.
21. Xu SH, Bo YH, Ma HC, Zhang HN and Shao MJ: lncRNA LINC00473 promotes proliferation, migration, invasion and inhibition of apoptosis of non-small cell lung cancer cells by acting as a sponge of miR-497-5p. Oncol Lett 21: 429, 2021.
22. Xu Y, Jiang Y, Wang Y, Zhao Z and Li T: LINC00473 rescues human bone marrow mesenchymal stem cells from apoptosis induced by dexamethasone through the PEBP1-mediated Akt/Bad/Bcl-2 signaling pathway. Int J Mol Med 47: 171-182, 2021.
23. Yeung K, Seitz T, Li S, Janosch P, McFerran B, Kaiser C, Fee F, Katsanakis KD, Rose DW, Mischak H, *et al*: Suppression of Raf-1 kinase activity and MAP kinase signalling by RKIP. Nature 401: 173-177, 1999.
24. Noh HS, Hah YS, Zada S, Ha JH, Sim G, Hwang JS, Lai TH, Nguyen HQ, Park JY, Kim HJ, *et al*: PEBP1, a RAF kinase inhibitory protein, negatively regulates starvation-induced autophagy by direct interaction with LC3. Autophagy 12: 2183-2196, 2016.
25. Zhang Y, Song X, Wang X, Hu J and Jiang L: Silencing of LncRNA HULC enhances chemotherapy induced apoptosis in human gastric cancer. J Med Biochem 35: 137-143, 2016.
26. Zhou Y, Zhang Y, Shao Y, Yue X, Chu Y, Yang C and Chen D: LncRNA HOTAIR down-expression inhibits the invasion and tumorigenicity of epithelial ovarian cancer cells by suppressing TGF-β1 and ZEB1. Discov Oncol 14: 228, 2023.
27. Casagrande N, Borghese C, Agostini F, Durante C, Mazzucato M, Colombatti A and Aldinucci D: In ovarian cancer multicellular spheroids, platelet releasate promotes growth, expansion of ALDH+ and CD133+ cancer stem cells, and protection against the cytotoxic effects of cisplatin, carboplatin and paclitaxel. Int J Mol Sci 22: 3019, 2021.
28. Ma N, Zhang M, Hu J, Wei Z and Zhang S: Daphnetin induces ferroptosis in ovarian cancer by inhibiting NAD(P)H:Quinone oxidoreductase 1 (NQO1). Phytomedicine 132: 155876, 2024.
29. Wojtowicz K and Nowicki M: The characterization of the sensitive ovarian cancer cell lines A2780 and W1 in response to ovarian CAFs. Biochem Biophys Res Commun 662: 1-7, 2023.
30. Li X, Guo Y, Xing Z, Gong T, Yang L, Yang T, Chang B, Wang X, Yu B and Guo R: ABT-737 increases cisplatin sensitivity through the ROS-ASK1-JNK MAPK signaling axis in human ovarian cancer cisplatin-resistant A2780/DDP cells. Oncol Rep 52: 122, 2024.
31. Wang DY, Li N and Cui YL: Long non-coding RNA CCAT1 sponges miR-454 to promote chemoresistance of ovarian cancer cells to cisplatin by regulation of surviving. Cancer Res Treat 52: 798-814, 2020.
32. Wang B, Liu M, Zhuang R, Jiang J, Gao J, Wang H, Chen H, Zhang Z, Kuang Y and Li P: Long non-coding RNA CCAT2 promotes epithelial-mesenchymal transition involving Wnt/β-catenin pathway in epithelial ovarian carcinoma cells. Oncol Lett 15: 3369-3375, 2018.
33. Wang H, Ge W, Jiang W, Li D and Ju X: SRPK1-siRNA suppresses K562 cell growth and induces apoptosis via the PARP-caspase3 pathway. Mol Med Rep 17: 2070-2076, 2018.
34. Li S, Lv C, Li J, Xie T, Liu X, Zheng Z, Qin Z, Hui X and Yu Y: LncRNA LINC00473 promoted colorectal cancer cell proliferation and invasion by targeting miR-195 expression. Am J Transl Res 13: 6066-6075, 2021.
35. Ding LN, Yu YY, Ma CJ, Lei CJ and Zhang HB: SOX2-associated signaling pathways regulate biological phenotypes of cancers. Biomed Pharmacother 160: 114336, 2023.
36. Liu C, Barger CJ and Karpf AR: FOXM1: A multifunctional oncoprotein and emerging therapeutic target in ovarian cancer. Cancers (Basel) 13: 3065, 2021.
37. Disis ML, Taylor MH, Kelly K, Beck JT, Gordon M, Moore KM, Patel MR, Chaves J, Park H, Mita AC, *et al*: Efficacy and safety of Avelumab for patients with recurrent or refractory ovarian cancer: Phase 1b results from the JAVELIN solid tumor trial. JAMA Oncol 5: 393-401, 2019.
38. Fu Y, Zhang Y, Cui J, Yang G, Peng S, Mi W, Yin X, Yu Y, Jiang J, Liu Q, *et al*: SNP rs12982687 affects binding capacity of lncRNA UCA1 with miR-873-5p: involvement in smoking-triggered colorectal cancer progression. Cell Commun Signal 18: 37, 2020.
39. Wang X, Zhang H, Yin S, Yang Y, Yang H, Yang J, Zhou Z, Li S, Ying G and Ba Y: lncRNA-encoded pep-AP attenuates the pentose phosphate pathway and sensitizes colorectal cancer cells to oxaliplatin. EMBO Rep 23: e53140, 2022.
40. Jiang J, Wang S, Wang Z, Cai J, Han L, Xie L, Han Q, Wang W, Zhang Y, He X and Yang C: HOTAIR promotes paclitaxel resistance by regulating CHEK1 in ovarian cancer. Cancer Chemother Pharmacol 86: 295-305, 2020.
41. Kielbik M, Szulc-Kielbik I and Klink M: Impact of selected signaling proteins on SNAIL 1 and SNAIL 2 expression in ovarian cancer cell lines in relation to cells' cisplatin resistance and EMT markers level. Int J Mol Sci 22: 980, 2021.